Microscopic theory of the noncontact van der Waals interaction: Application to layered systems

V. Despoja,* M. Šunjić, and L. Marušić†

Department of Physics, University of Zagreb, Bijenička 32, HR-10000 Zagreb, Croatia

(Received 20 June 2006; revised manuscript received 20 September 2006; published 18 January 2007)

In this paper we introduce an efficient method for the calculation of the noncontact van der Waals interaction between two metallic slabs of arbitrary thicknesses and densities. Because of the numerical resolution, the method enables the detailed examination of transition from the classical to the intermediate region of the vdW interaction. We also demonstrate how this new microscopic formulation reduces to the classical Lifshitz formula for the van der Waals interaction. This method is applied to calculate the interaction between various planar systems and compared with some previous results.

I. INTRODUCTION

Density functional theory (DFT) has been enormously successful in describing electronic properties of a variety of systems, including thin films and semi-infinite solids, molecules, small particles and even atoms, in spite of the rather drastic approximations (LDA, GGA) which omit a substantial part of the correlation effects. Fast development of the nanophysics requires improved description of the interaction between the components of such systems, e.g., nanolayers or nanowires, but it is also important in the studies of soft matter or biological systems. Interaction responsible for the stability of such systems is the weak van der Waals (vdW) interaction. However, DFT-LDA was much less successful in describing this interaction where the long and intermediate range effects come exclusively from the electronic long range correlation effects, and several efforts were made to extend the DFT method and construct new functionals that would include vdW interaction in such systems.

Starting point is usually the so-called adiabatic connection formula (ACF), which gives the ground state exchange-correlation energy of the system and can also be expressed in terms of the sum of ring diagrams. Furthermore, the summation of all unconnected ring diagrams can be performed by the integration over the coupling constant λ, which represents the strength of the coulomb interaction (i.e., the interaction Hamiltonian is written in the form $\lambda V(\mathbf{r}, \mathbf{r}')$ where V is the bare Coulomb interaction). This introduces additional difficulties, but ACF then becomes a simple functional of the response or dielectric function of the system. ACF also involves exact exchange-correlation density functional E_{xc}, and by use of the local approximation for the response or dielectric function it becomes an explicit functional of the local densities. This approach has been used, e.g., to calculate the interaction between two semi-infinite metals.[1] Also, a microscopic generalization of such a method (where the exchange correlation functional was divided into local and nonlocal part $E_{xc} = E_{xc}^{LDA/GGA} + E_{xc}^{nl}$) has been used to calculate the vdW interaction between two metallic films or semi-infinite metals, with their distance ranging from asymptotic separation to full contact.[2] Recently, nonlocal correlation functional has been used to give better description of the interaction between certain layered systems,[3] as well as to give the description of the dimerization of rare gas atoms and benzene

molecules.[4] Similar extension of the LDA approximations combine the ACF and the screening equation, using the independent particle KS response function or an approximation based on the homogeneous system (Lindhard) response function.[5] These approximate density functional methods are in good agreement with the exact RPA results at small and intermediate distances. This was rewarding, because these methods were numerically several hundred times more efficient than the exact RPA calculation. However, exact RPA calculation includes exact "nonlocality" and gives the details of the vdW interaction from the asymptotic to the contact region.[6] Moreover, because of the neglecting of the short-range correlations in the overlap regime there seems to be the need to go beyond RPA. However, it has been proven[7] that correction of the RPA results with exchange-correlation kernels f_{xc} (e.g., using the TDDFT form of the screening equation) gives the same results even in the overlap regime. Nevertheless, the effects beyond RPA are important in calculating the total or surface correlation energy.[8]

Details of the electronic structure also influence the behavior of the vdW interaction in the asymptotic region. For example, recently Dobson *et al.* discovered that anisotropic nanostructures, having zero electronic gap, such as metallic nanotubes or nanowires and nanolayered systems like metallic or graphene planes, do not show standard power law dependence in the asymptotic vdW region.[9]

On the other hand, classical theory of the van der Waals forces is well established, e.g., in the form of the Lifshitz formula which is based on the local (long wavelength) dielectric functions of the systems, ignoring quantum-mechanical character of the charge fluctuations. It was therefore plausible to extend the validity of the Lifshitz formula by replacing the classical reflectivity by its quantum mechanical analogon. It was soon discovered that the classical Lifshitz formula (via field matching) could be reproduced using ACF. Early attempts continued in this direction by using local SCIBM surface response function[10,11] or adding terms linear in the wave vector expansion of the dielectric function calculated within LDA.[1] Full nonlocal RPA calculation leads to serious numerical problems, therefore it was only applied to very thin, practically two-dimensional slabs.[5,6,8]

In this paper we modify previous theories of the van der Waals interaction, and develop a formulation which is almost exact for the planar systems with nonoverlapping charge

densities. We express the response function of the system consisting of two coupled slabs in terms of the response functions of individual slabs. The procedure is not restricted to RPA, and the response function of the total system includes all local field corrections due to intraslab Coulomb interaction, but not the local field corrections due to interslab coupling, which are expected to be small. Then we can perform the coupling constant integration analytically. The final result is given in terms of discrete matrices with the dimension which can be ten times smaller than in the analogous spatial matrices, so the numerical calculations are substantially faster. This enables us to perform accurate calculations of vdW interaction at large separations. Comparing this with the previous calculations, we can also evaluate the separation at which the overlap of electron densities begins to influence the results. It is also demonstrated that the new expression in the local approximation directly reduces to the Lifshitz formula.

In Sec. II we obtain the quantum-mechanical expression for the vdW interaction between planar systems in terms of response functions of separate systems, calculated in the best possible way, without any restriction on the method. In Sec. III we show how this expression reduces to the classical Lifshitz formula if we replace the surface excitation propagator by the surface reflectivity. We also show how to perform a complex integration (slightly modified with respect to Ref. 12) by which we express the vdW energy as the sum of differences between coupled and uncoupled surface excitation frequencies. In Sec. IV we show how our method can be applied to the calculation of vdW interaction for metallic films of various thicknesses and densities. Results for interaction between two very thin metallic films at short distances are compared with those obtained in Ref. 6. We show that the $d^{-5/2}$ power law[9] remains valid for any finite film thickness.

II. FORMULATION OF THE PROBLEM

We shall consider two subsystems with nonoverlapping charge densities, described by the Hamiltonian

$$H = H_1 + H_2 + \lambda H_{int}, \tag{1}$$

where $\lambda \in [0,1]$ and Hamiltonian $H_i (i=1,2)$ of each subsystem consists of kinetic energy, interaction with the crystal lattice of the subsystem (or homogeneous background if the *jellium* model is used), and electron-electron interaction within the subsystem. The interaction between the subsystems is

$$H_{int} = \int_{V_1} d\mathbf{r} \int_{V_2} d\mathbf{r}' n_1(\mathbf{r}) v_{12}(\mathbf{r},\mathbf{r}') n_2(\mathbf{r}'), \tag{2}$$

where $n_{1,2}$ are the charge density operators in the subsystems and v_{12} is the bare inter-subsystem coulomb interaction. Note that H_{int} can be written in this form because, due to the fact that the electron densities of the slabs do not overlap, $n_1(\mathbf{r}) v_{12}(\mathbf{r},\mathbf{r}') n_2(\mathbf{r}') = n_2(\mathbf{r}) v_{21}(\mathbf{r},\mathbf{r}') n_1(\mathbf{r}')$. If there is no interaction between the subsystems ($\lambda=0$) the exact ground state of the system is $\psi_0(\lambda=0)$. With the interaction included ($\lambda \neq 0$) the exact ground state is $\psi_0(\lambda)$, and the total ground state energy is

$$E_0 = \langle \psi_0(\lambda) | H_1 + H_2 + \lambda H_{int} | \psi_0(\lambda) \rangle. \tag{3}$$

A. Derivation of $E_c(d)$

Using the standard Pauli trick the ground state energy of the fully interacting system ($\lambda=1$) can be written as

$$E_0 = E_0(\lambda = 0) + \int_0^1 \frac{d\lambda}{\lambda} E_{int}(\lambda), \tag{4}$$

where

$$E_{int}(\lambda) = \langle \psi_0(\lambda) | \lambda H_{int} | \psi_0(\lambda) \rangle. \tag{5}$$

$E_0(\lambda=0)$ is the sum of exact ground state energies of the two noninteracting subsystems ($\lambda=0$). The ground state energy shift to the coupling between the subsystems (i.e., interaction energy) is therefore

$$E_c = \int_0^1 \frac{d\lambda}{\lambda} E_{int}(\lambda). \tag{6}$$

This energy is due to the correlation because for nonoverlapping systems complete exchange (for each subsystem) is already included in $E_0(\lambda=0)$. Assuming that the ground state energies of separate subsystems are already evaluated, let us study the change in the total energy when the interaction is included. Inserting (2) and (5) in (6) gives

$$E_c = \int_0^1 \frac{d\lambda}{\lambda} \int_{V_1} d\mathbf{r} \int_{V_2} d\mathbf{r}' v_\lambda^{12}(\mathbf{r},\mathbf{r}')$$
$$\times \langle \psi_0(\lambda) | n_1(\mathbf{r}) n_2(\mathbf{r}') | \psi_0(\lambda) \rangle, \tag{7}$$

where $v_\lambda^{12}(\mathbf{r},\mathbf{r}') = \lambda e^2 / |\mathbf{r} - \mathbf{r}'|$.

The matrix element in (7) can be related to the correlation function of the system. Namely, for nonoverlaping subsystems the density operator can be written in the form $n(\mathbf{r}) = n_1(\mathbf{r}) + n_2(\mathbf{r})$ and the correlation function $S_\lambda(\mathbf{r},\mathbf{r}',t=0,t'=0)$ consists of four terms: S^{11}, S^{12}, S^{21}, and S^{22}, given by

$$S_\lambda^{ij}(\mathbf{r},\mathbf{r}',0,0) = \langle \psi_0(\lambda) | n_i(\mathbf{r}) n_j(\mathbf{r}') | \psi_0(\lambda) \rangle, \quad i=1,2, \tag{8}$$

where $n_i(\mathbf{r})$ is the density operator in subsystem i. Only the term S_λ^{12} (which is, because the electron densities of the slabs do not overlap, equal to S_λ^{21}) appears in the integration in (7), and by use of the relation:

$$S_\lambda^{12}(\mathbf{r},\mathbf{r}',t=0,t'=0) = -\frac{1}{\pi} \text{Im} \int_0^\infty d\omega R_\lambda^{12}(\mathbf{r},\mathbf{r}',\omega) \tag{9}$$

(7) becomes

$$E_c = -\frac{1}{\pi} \text{Im} \int_{V_1} d\mathbf{r} \int_{V_2} d\mathbf{r}' \int_0^\infty d\omega \int_0^1 \frac{d\lambda}{\lambda}$$
$$\times v_\lambda^{21}(\mathbf{r},\mathbf{r}') R_\lambda^{12}(\mathbf{r},\mathbf{r}',\omega) \tag{10}$$

Here R_λ^{12} is the response function between the points $\mathbf{r}$ and $\mathbf{r}'$, located in different subsystems. A detailed description of the calculation of the response functions for the two sub-
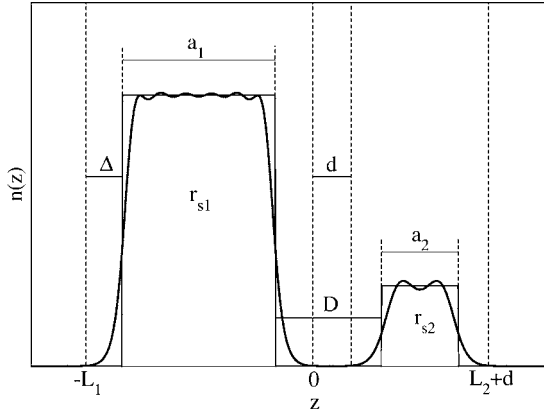
FIG. 1. Density profile for two nonoverlapping metallic slabs.

systems can be found in Ref. 13. The integrand in (10) represents the sum of all connected ring diagrams for the ground state energy shift. The coupling constant integration enables us to express all the diagrams for ground state fluctuations in terms of the connected ones.[14]

B. Application to planar systems

To consider the van der Waals interaction between two parallel metallic slabs (Fig. 1) we assume one of the slabs in the region $-L_1 \leq z \leq 0$ with electron density corresponding to r_{s1}, and the other one in the region $d \leq z \leq d+L_2$ with electron density corresponding to r_{s2}. In other words d is the distance between the points where the electron densities of the two slabs practically vanish, while the distance between jellium edges is $D = d + 2\Delta$ (Fig. 1), where Δ is the characteristic electron density decay length. The jellium thicknesses are then $a_1 = L_1 - 2\Delta$ and $a_2 = L_2 - 2\Delta$.

Now we can use translational symmetry parallel to the surface and Fourier transform Eq. (10):

$$\frac{E_c(d)}{A} = -\frac{1}{\pi} \text{Im} \int_{-L_1}^{0} dx \int_{d}^{L_2+d} dy \int_0^{\infty} d\omega \int \frac{d\mathbf{Q}}{(2\pi)^2} \int_0^1 \frac{d\lambda}{\lambda}$$
$$\times R_\lambda^{12}(\mathbf{Q}, x, y, \omega) v_\lambda^{21}(\mathbf{Q}, y, x), \quad (11)$$

where

FIG. 2. Dyson series for $R_\lambda^{12}(\mathbf{Q}, \omega, z, z')$, as in Eq. (15).

$$v_\lambda^{21}(\mathbf{Q}, y, x) = \lambda v_Q e^{-Q(y-x)}; \quad v_Q = \frac{2\pi e^2}{Q}. \quad (12)$$

$\mathbf{Q}$ is the wave vector parallel to the surface, A is the surface area, and points x and y are located in the left slab (subsystem 1) and the right slab (subsystem 2), respectively.

Following the procedure presented in Ref. 13 we can transform the integral equation (11) into the matrix equation:

$$\frac{E_c(d)}{A} = -\frac{1}{\pi} \text{Im} \int_0^{\infty} d\omega \int \frac{d\mathbf{Q}}{(2\pi)^2} \int_0^1 \frac{d\lambda}{\lambda} Tr\{\mathbf{R}_\lambda^{12} \mathbf{v}_\lambda^{21}\}. \quad (13)$$

Calculation of the the matrix elements of $\mathbf{R}_\lambda^{12}$ are presented in detail in the following subsection and $\mathbf{v}_\lambda^{12}$ are

$$\mathbf{v}_{\lambda,q_1 q_2}^{12} = \tilde{\mathbf{v}}_{\lambda,q_1 q_2}^{12} e^{-Qd}$$
$$= \lambda \frac{8\pi e^2 Q}{L_1 L_2} \eta_{q_1} \eta_{q_2} \frac{(1 - p_{q_1} e^{-QL_1})(1 - p_{q_2} e^{-QL_2})}{(q_1^2 + Q^2)(q_2^2 + Q^2)} e^{-Qd}, \quad (14)$$

where p_{q_i} is the parity of q_i-th cosine harmonic, i.e., $p_{q_i} = (-)^{q_i L_i / 2\pi}$.

C. Van der Waals interaction between two slabs

First we want to write the response function connecting two slabs $R_\lambda^{12}(\mathbf{Q}, x, y, \omega)$ (with point x being in slab 1 and point y being in slab 2) in terms of the response functions R^1 and R^2 of the individual slabs. To achieve that we examine the following integral equation:[13]

$$R_\lambda^{12}(\mathbf{Q}, x, y, \omega) = \Pi_\lambda(\mathbf{Q}, x, y, \omega) + \int_{-L_1}^{0} dx_2 \int_{d}^{L_2+d} dy_2 \Pi_\lambda(\mathbf{Q}, x, y_2, \omega) v_\lambda^{21}(\mathbf{Q}, y_2, x_2) \Pi_\lambda(\mathbf{Q}, x_2, y, \omega) + \cdots \quad (15)$$

where the first term is

$$\Pi_\lambda(\mathbf{Q}, x, y, \omega) = \int_{-L_1}^{0} dx_1 \int_{d}^{L_2+d} dy_1 R_\lambda^1(\mathbf{Q}, x, x_1, \omega) v_\lambda^{12}(\mathbf{Q}, x_1, y_1) R_\lambda^2(\mathbf{Q}, y_1, y, \omega) \quad (16)$$
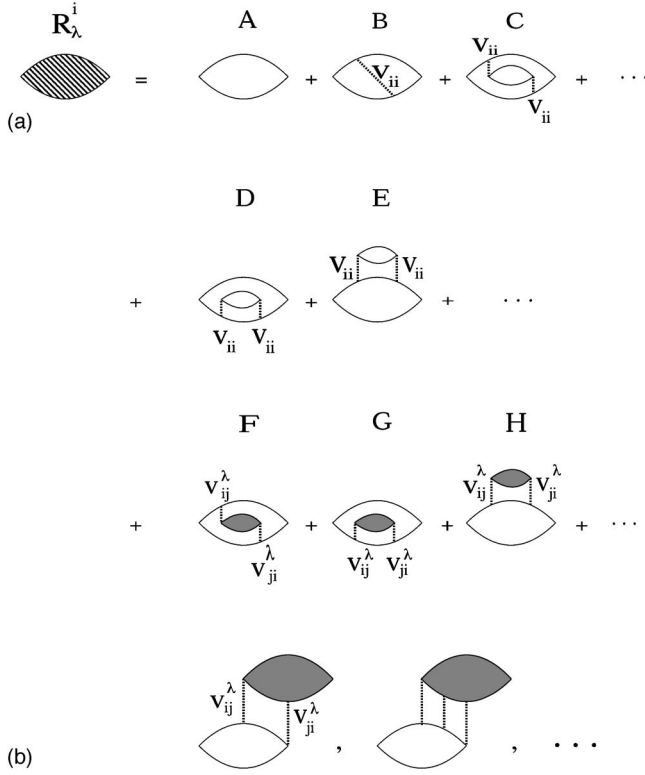
FIG. 3. (a) Series expansion for the response function R^i_λ of the slab i: A- RPA term; B and C- local field intraslab vertex corrections; D and E- local field intraslab self-energy corrections; F- local field interslab vertex corrections; G and H- local field interslab self-energy corrections. Black bubbles denote possible diagrams in the expansion for R^j_λ. (b) diagrams containing the nonlinear interslab terms for which the starting and the final points are in different slabs.

as shown in Fig. 2. Here the points x and x_1 can obviously be located only inside the slab 1 while the points y and y_1 can only be within the slab 2 which means that R^1_λ and R^2_λ are the response functions describing the situation where the the starting and the final point are both inside the same slab [as shown in Fig. 3(a)], but not the situation where the starting and the final points are in different slabs. In other words, this formulation is almost exact, and neglects only the diagrams like the ones shown in Fig. 3(b). In order to perform the λ integration in (13) analytically, we make further approximation, and neglect the diagrams F, G, and H [Fig. 3(a)] and similar, containing the interslab local field corrections mediated by v^{12}_λ and v^{21}_λ. This way, instead of having the response functions R^1_λ and R^2_λ we have reduced the formulation to the response functions R^i, which are the exact response functions of the completely separate slabs and do not contain the coupling constant λ. This approximation is obviously well justified in the situation where the electronic densities of the slabs do not overlap, since in that case the interslab local field corrections are very small. However, this formulation is by no means restricted to RPA, since all the intraslab local-field corrections, such as those shown in diagrams B, C, D, and E, are still included.

After transforming (15) and (16) into matrix form, $\mathbf{R}^{12}_\lambda$ can be expressed as
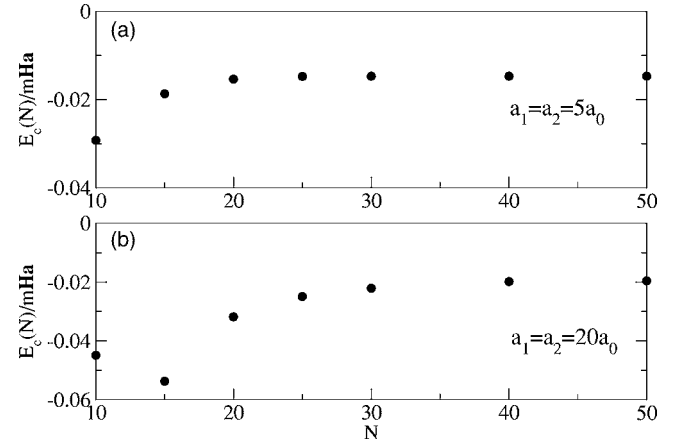

FIG. 4. Convergence of the vdW energies at fixed film separation $D=12a_0$ for two film thicknesses (a) $a_1=a_2=5a_0$ and (b) $a_1=a_2=20a_0$, as functions of the number of cosine harmonics ($r_{s1}=r_{s2}=2$).

$$\mathbf{R}^{12}_\lambda = \mathbf{\Pi}_\lambda + \mathbf{\Pi}_\lambda \mathbf{v}^{21}_\lambda \mathbf{\Pi}_\lambda + \cdots = (\mathbf{1} - \mathbf{\Pi}_\lambda \mathbf{v}^{21}_\lambda)^{-1} \mathbf{\Pi}_\lambda, \quad (17)$$

where $\mathbf{\Pi}_\lambda = \mathbf{R}_1 \mathbf{v}^{12}_\lambda \mathbf{R}_2$. Inserting (17) into (13) and using symmetry properties $\mathbf{v}^{21}_\lambda = \mathbf{v}^{12T}_\lambda$ gives

$$\frac{E_c(d)}{A} = -\frac{1}{\pi} \, \mathrm{Im} \int_0^\infty d\omega \int \frac{d\mathbf{Q}}{(2\pi)^2} \int_0^1 \frac{d\lambda}{\lambda}$$
$$\times Tr\{(\mathbf{1} - \mathbf{\Pi}_\lambda \mathbf{v}^{12T}_\lambda)^{-1} \mathbf{\Pi}_\lambda \mathbf{v}^{12T}_\lambda\}. \quad (18)$$

To perform the λ integration we introduce the notation $\mathbf{\Pi}_\lambda \mathbf{v}^{12T}_\lambda = \lambda^2 \mathbf{A}$ and use the mathematical identity $Tr\{\ln(1-\mathbf{A})\} = \ln\{\det(1-\mathbf{A})\}$ and obtain

$$\frac{E_c(d)}{A} = \mathrm{Im} \int \frac{d\mathbf{Q}}{(2\pi)^2} \int_0^\infty \frac{d\omega}{2\pi} \ln\{\det(\mathbf{1} - e^{-2Qd}\mathbf{R}_1 \tilde{\mathbf{v}}^{12} \mathbf{R}_2 \tilde{\mathbf{v}}^{12T})\},$$
$$(19)$$

where $\tilde{\mathbf{v}}^{12}$ is defined in (14). This expression, which is actually the microscopic analogon of the Lifshitz formula, as will be shown in Sec. III, has several advantages. The key quantity is the matrix $\mathbf{M} = \mathbf{R}_1 \tilde{\mathbf{v}}^{12} \mathbf{R}_2 \tilde{\mathbf{v}}^{12T}$, which is independent of the slab separation d, so for each Q and ω the matrix $\mathbf{M}$ must be calculated only once. For thicker slabs or semi-infinite metals the dimension of the matrix $\mathbf{M}$ does not need to be more than fifty, regardless of the distance between the slabs. For thinner slabs like those in Refs. 5–7 the dimension of the matrix $\mathbf{M}$ does not need to exceed 25.

As an illustration, in Fig. 4 we demonstrate the fast convergence of the correlation energy E_c (for a fixed slab separation) with respect to the dimension of the matrices. Clearly, for slab thicknesses $a_1=a_2=5a_0$ and separation $D=12a_0$ the result converges already for $N=25$, for slab thicknesses $a_1=a_2=20a_0$ and the same separation for $N=40$. At larger separations convergence is still faster.

It is important to notice that the coupling constant integration was performed analytically, regardless of how the matrices $\mathbf{R}_i$ are calculated. For example, in the TDDFT method to evaluate $\mathbf{R}_i$:

$$\mathbf{R}_i = \mathbf{R}_i^{KS} + \mathbf{R}_i^{KS}(\mathbf{v}_i + \mathbf{f}_{xc})\mathbf{R}_i \qquad (20)$$

we can correct $\mathbf{v}_i$ by the various forms of the exchange-correlation kernels $\mathbf{f}_{xc}$, which would correspond to adding the intraslab local field corrections (as discussed in Sec. II), without increasing numerical difficulty in (19). Including the interslab correction terms presented, e.g., in Fig. 3 (and neglected in the procedure presented in this paper), would contribute little, because they are reduced at least by the factor e^{-2Qd}, and could become important only for finite overlap. In conclusion, we consider that this method is about hundred times faster than the existing numerical methods, and probably comparable to some fast DF approaches like those in Ref. 2.

III. CLASSICAL LIMIT

A. Alternative expression for the van der Waals energy

Instead of working with matrices in the final expression (19) we notice that the right-hand side of (11) contains the expression of the form:

$$\int_{-L_1}^{0} dx \int_{d}^{L_2+d} dy R_\lambda^{12}(\mathbf{Q},x,y,\omega) v_\lambda^{21}(\mathbf{Q},y,x) \qquad (21)$$

which, with use of (15) can be written in terms of the integrated quantities

$$v_Q \int_{-L_1}^{0} dx_1 \int_{-L_1}^{0} dx_2 e^{Qx_1} R_\lambda^{1}(\mathbf{Q},x_1,x_2,\omega) e^{Qx_2} = D_1(\mathbf{Q},\omega) \qquad (22)$$

and similarly for $D_2(\mathbf{Q},\omega)$. By use of that, Eq. (19) can be rewritten as[15]

$$\frac{E_c(d)}{A} = \mathrm{Im} \int \frac{d\mathbf{Q}}{(2\pi)^2} \int_0^\infty \frac{d\omega}{2\pi}$$
$$\times \ln[1 - e^{-2Qd} D_1(\mathbf{Q},\omega) D_2(\mathbf{Q},\omega)]. \qquad (23)$$

From Eq. (22) we can see that D_i is in fact the surface excitation propagator,[13,16–18] which can be related to the surface dielectric functions $\epsilon_p(\mathbf{Q},\omega) = \epsilon_p(\mathbf{Q},\omega,0,0)$.

$$D_i(\mathbf{Q},\omega) = \frac{1}{v_Q} W_i^{ind}(\mathbf{Q},\omega,z=0,z'=0) = \frac{1}{2}\sum_{p=\pm1} D_{i,p}(\mathbf{Q},\omega),$$
$$i = 1,2, \qquad (24)$$

where

$$D_{i,p}(\mathbf{Q},\omega) = \frac{c_p - c_{-p}\epsilon_p(\mathbf{Q},\omega)}{1 + \epsilon_p(\mathbf{Q},\omega)}, \quad c_p = 1 - pe^{-QL_i} \qquad (25)$$

and p denotes the parity of the single slab surface excitations. We need to emphasize that evaluating vdW energy from expressions (19) or (23), requires the same numerical effort: in the first case matrix multiplication, in the latter evaluation of matrix sums for D_i's. Therefore, in Sec. IV we use the first expression.

B. Lifshitz formula

It is now easy to verify that the microscopic expressions (19) and (23) give the expected results in the classical limit. We consider the case of two semi-infinite solids separated by the distance d. For semi-infinite solids surface excitation propagators have the similar form like (25) but do not depend on parity, i.e., $p=0$.[17,18] In the clasical limit surface dielectric function $\epsilon(\mathbf{Q},\omega)$ is replaced by the bulk (local) dielectric function $\epsilon(\Omega)$ where $\Omega = \omega + i\eta \, \mathrm{sgn}(\omega)$. So, the surface excitation propagators transform into

$$D_i(\mathbf{Q},\omega) \rightarrow \frac{1 - \epsilon_i(\Omega)}{1 + \epsilon_i(\Omega)} = r_i^S(\Omega), \quad i = 1,2 \qquad (26)$$

and can be recognized as the surface reflectivity functions r_i^S. In the classical limit the electronic charge density distribution edges correspond to the jellium edges, i.e., $\Delta \rightarrow 0$, so $d \rightarrow D$ and $L_i \rightarrow a_i$, $i=1,2$ (Fig. 2), leading to

$$\frac{E_c(D)}{A} = -\frac{1}{2}\int \frac{d\mathbf{Q}}{(2\pi)^2} \oint \frac{d\omega}{2\pi i} \times \ln\{1 - r_1^S(\Omega) r_2^S(\Omega) e^{-2QD}\}, \qquad (27)$$

where the frequency integration is extended to the complex ω plane and the contour of integration is a semicircle in the lower part of the complex ω-plane. Equation (27) is the well-known Lifshitz formula for the van der Waals interaction between two metallic surfaces.

In a similar way we can find the classical limit of our result (19) for the interaction between two different metallic slabs with thicknesses a_i. Surface excitation propagators (24) and (25) are then replaced by the surface reflectivities of the slabs:

$$D_i(\mathbf{Q},\Omega) \rightarrow r_i^F(Q,\Omega) = r_i^S(\Omega) \frac{1 - e^{-2Qa_i}}{1 - [r_i^S(\Omega)]^2 e^{-2Qa_i}}. \qquad (28)$$

Equation (27) with the modified reflectivities $r_i^S \rightarrow r_i^F$ given by (28) is exactly the classical limit of our quantum-mechanical results (19) and (23).

C. Van der Waals energy and zero point energies

One can transform the Lifshitz formula (27) by performing the frequency integration and express the van der Waals energy in terms of the differences of zero point energies of the coupled and separate slabs.[12] After partial integration in (27) we can apply the Rouche' theorem, valid for any meromorphic function $f(z)$ (has no singularity except poles) and any analytic function $g(z)$ inside the positive contour of integration Γ:

$$\frac{1}{2\pi i}\oint_\Gamma dz g(z)\frac{d}{dz}\ln f(z) = \sum_{i=1}^{N_z} n_i g(a_i) - \sum_{i=1}^{N_p} m_i g(b_i),$$

where $\{a_i\}$ are zeros of the order $\{n_i\}$ and $\{b_i\}$ are poles of the order $\{m_i\}$ of the function $f(z)$ inside the contour of integration Γ. Zeros of the function:
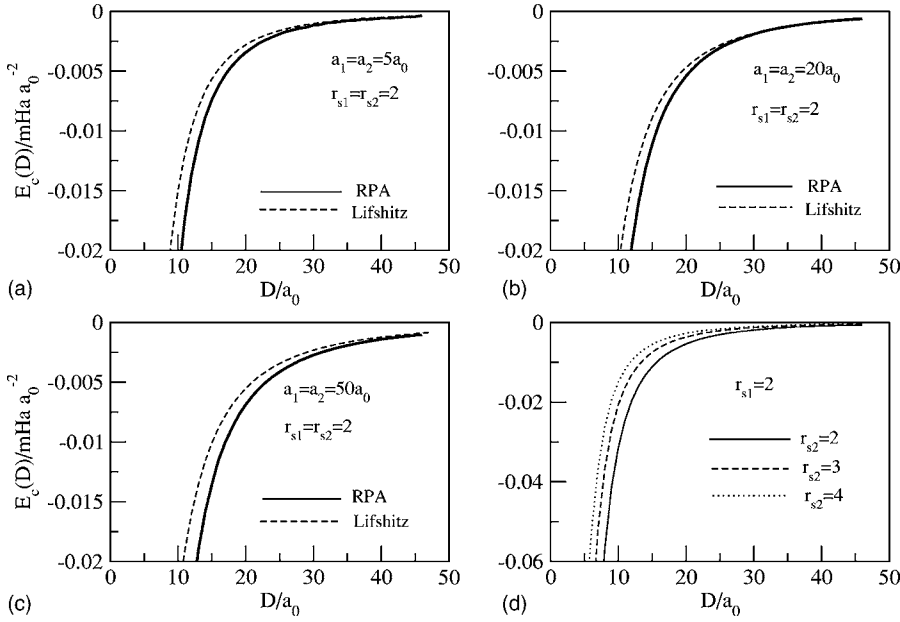
FIG. 5. Quantum mechanical van der Waals energy per unit area between two metallic slabs (a) $r_{s1}=r_{s2}=2.07$ and $a_1=a_2=5a_0$; (b) $r_{s1}=r_{s2}=2$ and $a_1=a_2=20a_0$; (c) $r_{s1}=r_{s2}=2$ and $a_1=a_2=50a_0$; (d) $a_1=a_2=20a_0$ and $r_{s1}=r_{s2}=2$ (full line), $r_{s1}=2$, $r_{s2}=3$ (dashed line), $r_{s1}=2$, $r_{s2}=4$ (dotted line).

$$f(\Omega) = 1 - r_1^S(\Omega) r_2^S(\Omega) e^{-2QD}$$

are the frequencies of the two surface plasmon modes of the coupled semi-infinite solids $\omega_i(Q,D)$. Poles of $f(\Omega)$ are the poles of the reflectivities r_i, which correspond to the asymptotic surface plasmon frequencies $\omega_i = \omega_i(Q,D\rightarrow\infty)$ of the two separated semi-infinite solids. Integrating (27) in the complex ω plane gives

$$\frac{E_c(D)}{A} = \frac{1}{2}\sum_{i=1,2}\int\frac{d\mathbf{Q}}{(2\pi)^2}[\omega_i(Q,D) - \omega_i(Q,D\rightarrow\infty)].$$

$$(29)$$

IV. QUANTUM-MECHANICAL CALCULATIONS

To perform the quantum mechanical calculation of the vdW interaction between two metallic slabs we use the expression (19) which we compare with the classical result (29). Let us describe the steps in the calculation of the vdW interaction between two metallic slabs using formula (19).

1. Calculation of the matrices R_i

We first transform the KS-response functions R_i^{KS} (Refs. 13 and 18) into the matrices. Solving the Dyson equation:

$$\mathbf{R}_i = \mathbf{R}_i^{KS} + \mathbf{R}_i^{KS}(\mathbf{v}_i + \mathbf{f}_{xc})\mathbf{R}_i$$

by using simple Gauss-Jordan method for the matrix inversion we obtain matrices $\mathbf{R_i}$. Form of the matrices $\mathbf{v}_i$ can be found in Ref. 13. We restrict our calculation to RPA, so we put the $\mathbf{f}_{xc}$ matrix to be zero. Dimension of the matrix $\mathbf{R_i}$ depends on the slab thickness, but not significantly. For slab thickness $5a_0$ it is 25 and for semiinfinite metals it is 50.

2. Calculation of the determinant

First we construct the matrix

$$\mathbf{M} = \mathbf{R}_1\tilde{\mathbf{v}}^{12}\mathbf{R}_2\tilde{\mathbf{v}}^{12T}$$

$$(30)$$

and then for every d the matrix

$$\mathbf{F} = \mathbf{1} - e^{-2Qd}\mathbf{M}.$$

$$(31)$$

Matrix $\mathbf{F}$ is then transformed into the upper triangle matrix, and the summation of the logarithms of the diagonal elements gives the function

$$f = \ln[\det\mathbf{F}].$$

$$(32)$$

3. Q integration

Function f in (32) is very smooth function of Q, so we use simple Simpson integration. The interval of integration depends on the separation between slabs because the contributions to vdW interaction go as e^{-2QD}, which at the same time defines the characteristic cutoff. So, e.g., for the separation $D=8a_0$ the interval of integration is $Q=0.005-1.0a_0^{-1}$ with maximally fifty points used for integration.

4. ω integration

ω integration is the greatest problem in the evaluation of E_c at large separations d. For small Q the function f has four sharp peaks which originate from four surface plasmons and which give dominant contributions at large d. If we want to calculate vdW interaction precisely we must integrate carefully around these sharp peaks at the energies that also depend on the separation d.

It is well known that one could also transform the expressions (19) and (23) into the form which is easier for ω integration, though it is less physically transparent. We replace $\omega\rightarrow iu$, in order to exploit the fact that the response functions in (19) and (23) are real and smooth (with no peaks) functions on the imaginary axis.

For comparison we shall also evaluate the classical results using the expression (29). In the classical limit the function f transforms into

$$f = 1 - r_1^F(Q,\Omega) r_2^F(Q,\Omega) e^{-2QD},$$

where $r_i^F(Q,\Omega)$ are surface reflectivities for the slabs given by (28). Now the frequency integration can be performed analytically and expressed in the form of the differences be-
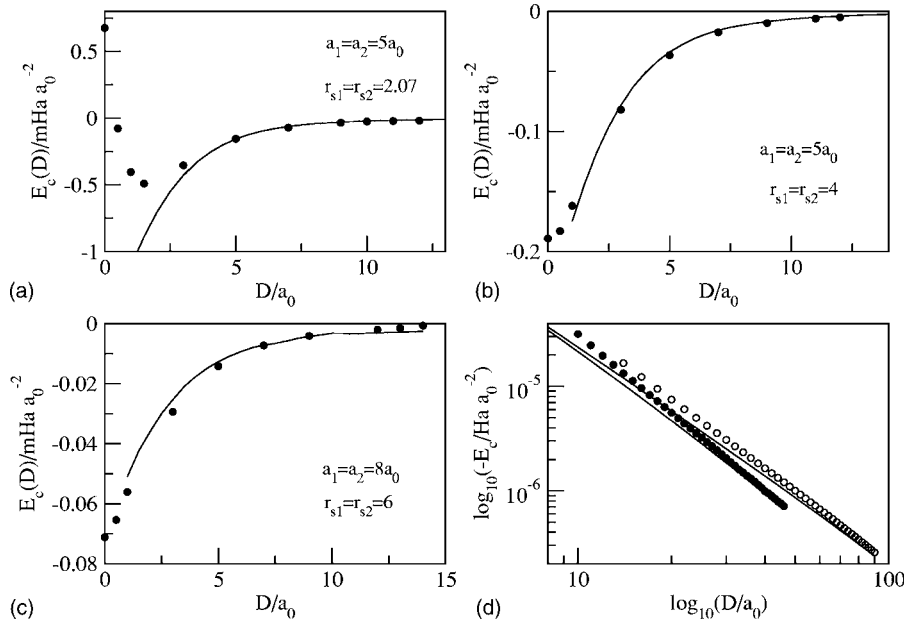
FIG. 6. Quantum mechanical van der Waals energy per unit area (full line) between (a)two metallic slabs $r_{s1}=r_{s2}=2.07$ and $a_1=a_2=5a_0$; (b)two metallic slabs $r_{s1}=r_{s2}=4$ and $a_1=a_2=5a_0$; (c)two metallic slabs $r_{s1}=r_{s2}=6$ and $a_1=a_2=8a_0$; dots are nonlocal RPA calculations from Ref. 6; (d)Illustration of the power-law behavior of vdW energy: full lines correspond to classical (varying from d^{-2} to $d^{-5/2}$) dependence, quantum calculations are shown by dots $(a_1=a_2=20a_0)$ and circles $(a_1=a_2=100a_0)$.

tween zeros and poles of the function f, as in (29). So the only problem is Q integration of the differences between the four coupled plasmon frequencies $\omega_i(D,Q)$, which are the solutions of the equation

$$r_1^F(Q,\omega)r_2^F(Q,\omega)e^{-2QD} = 1,$$

and four uncoupled plasmons frequencies

$$\omega_{1,2}(Q,D \to \infty) = \frac{\omega_{p,i}}{\sqrt{2}}\sqrt{1 \pm e^{-Qa_i}}$$

(where the $\omega_{p,i}$ are the bulk plasma frequencies) which are solutions of the equation

$$r_i^F(Q,\omega) = \infty; \quad i = 1,2.$$

V. DISCUSSION OF THE RESULTS

Here we want to illustrate briefly the application of the microscopic expressions (19) and (23) for the van der Waals energies, with the results presented in Fig. 5 and Fig. 6. Figures 5(a)–5(c) show the vdW interaction between slabs of various thicknesses and are compared with the classical (Lifshitz) results. Strength of the vdW interaction and its deviation from the classical results at intermediate distances (10 to $40a_0$) increase with slab thickness. The number of occupied electronic subbands for slab thicknesses 5, 20, and $50a_0$ presented in Figs. 5(a)–5(c) are 2, 7 and 16, respectively.

Figure 5(d) represents the vdW interaction between slabs for different slab densities. As the difference between densities (plasmon frequencies) increases, the strength of the vdW interaction decreases, because the coupling between surface charge oscillations, which gives the dominant contribution to the vdW interaction, goes "off-resonance."

In Figs. 6(a)–6(c), we compare our results with the "non-local" RPA results for vdW interaction between metallic slabs presented in Ref. 6 with the intention to examine the accuracy of our results at short distances. From Figs. 6(a)–6(c) it is obvious that our results are in very good agreement with those in Ref. 6 all the way to $D \approx 5a_0$ when the overlap becomes important. One could infer that our approach can be used even at small distances which would simplify the calculations.

Our approach also enables us to provide accurate vdW interaction in the asymptotic region $(d \to \infty)$. Figures 5(a)–5(c) show that the quantum-mechanical results in the asymptotic region approach the classical (Lifshitz) results. Also, vdW interaction for finite slab thicknesses shows some interesting behavior. As shown by Dobson,[9] for 2D layers it varies as $d^{-5/2}$, and we verify that this is true for finite L both in the classical and quantum-mechanical calculations [Fig. 6(d)]. In fact, d^{-2} behavior cannot be obtained for any finite L.

In conclusion, our new formulation provides an efficient method for further calculations of the quantum-mechanical vdW interaction between planar systems with nonoverlapping charge densities, and enables us to examine in detail quantum mechanical corrections to the classical results in the asymptotic region.

*Electronic address: vito@phy.hr

†Department of Transport and Maritime Studies, University of Zabar, M. Pavlinovića b.b., HR-23000 Zadar, Croatia.

[1] Y. Andersson *et al.*, Solid State Commun. **106**, 235 (1998).

[2] H. Rydberg, B. I. Lundqvist, D. C. Langreth, and M. Dion, Phys. Rev. B **62**, 6997 (2000).

[3] H. Rydberg *et al.*, Phys. Rev. Lett. **91**, 126402 (2003).

[4] M. Dion *et al.*, Phys. Rev. Lett. **92**, 246401 (2004).

[5] J. F. Dobson and J. Wang, Phys. Rev. Lett. **82**, 2123 (1999).

[6] J. F. Dobson and J. Wang, Phys. Rev. B **69**, 235104 (2004).

[7] J. F. Dobson and J. Wang, Phys. Rev. B **62**, 10038 (2000).

[8] J. Jung, P. Garcia-Gonzalez, J. F. Dobson, and R. W. Godby, Phys. Rev. B **70**, 205107 (2004).

[9] J. F. Dobson, A. White, and A. Rubio, Phys. Rev. Lett. **96**, 073201 (2006).

[10] J. Heinrichs, Phys. Rev. B **11**, 3625 (1975).

[11] J. Harris and A. Griffin, Phys. Rev. B **11**, 3669 (1975).

[12] N. G. van Kampen, B. R. A. Nijboer, and K. Schram, Phys. Lett. **26A**, 307 (1968).

[13] V. Despoja, L. Marušić, and M. Šunjić, J. Phys.: Condens. Matter **18**, 8217 (2006).

[14] G. D. Mahan, *Many-Partice Physics*, 2nd ed. (Plenum, New York, 1981) Sec. 3.6.

[15] An equvivalent result was obtained by Sernelius and Björk [B. E. Sernelius and P. Björk, Phys. Rev. B **57**, 6592 (1998)] for the special case of strictly two-dimensional metallic sheets and restricted to the RPA in each sheet.

[16] D. M. Newns, Phys. Rev. B **1**, 3304 (1970).

[17] Z. Penzar and M. Šunjić, Phys. Scr. **30**, 431 (1984).

[18] L. Marušić and M. Šunjić, Phys. Scr. **63**, 336 (2001).